Research Article | Vol. 10, No. 3 | 1 Mar 2019 | BIOMEDICAL OPTICS EXPRESS 1196
Biomedical Optics EXPRESS

Label-free self-referenced sensing of living cells by terahertz metamaterial-based reflection spectroscopy

XIANG ZHAO,[1] ZHONGQUAN LIN,[1] YUNXIA WANG,[1] XIANG YANG,[1] KE YANG,[1] YANG ZHANG,[1] JIA PENG,[1] MARC LAMY DE LA CHAPELLE,[2] LIQUN ZHANG,[3] AND WEILING FU[1,*]

[1]*Department of Laboratory Medicine, Southwest Hospital, Third Military Medical University (Army Medical University), Chongqing 400038, China*
[2]*Institut des Molécules et Matériaux du Mans (IMMM - UMR CNRS 6283), Le Mans Université, Avenue Olivier Messiaen, 72085 Le Mans cedex 9, France*
[3]*Department of Laboratory Medicine, Xinqiao Hospital, Third Military Medical University (Army Medical University), Chongqing 400038, China*
[*]*weiling_fu@126.com*

Abstract: Terahertz (THz) metamaterial-based reflection spectroscopy is proposed for label-free sensing of living cells by a self-referenced method. When sensing the living Madin-Darby canine kidney cell monolayer and phosphate buffered saline solution, self-referenced signals showed significant differences in peak intensity because of inherent discrepancy in the imaginary part of their complex refractive indices, as confirmed by 3D-FDTD simulations. The resonance peak intensity was unaffected by cell monolayer thickness variation, demonstrating feasibility for sensing various cells. Simulations and experiments showed that saponin-induced changes in cell permeability could be monitored in real-time. The self-referenced signal was linearly dependent on the adherent cell density, illustrating a label-free *in situ* THz metamaterial-based cell sensor.

1. Introduction

Cells, the fundamental unit of life, determine the structure and function of all living organisms. Thus, to comprehensively understand the proliferation, differentiation, interaction, and apoptosis of cells will further boost the development of research in bioscience and biomedicine. The biophysical properties of cells, including their mechanical [1], electrical [2] and optical properties [3], could provide a comprehensive perspective about how they function. Optical biosensing, a widely used non-invasive method, utilizes the passing of light through cells and measures the absorption, reflection, and scattering coefficient, which helps obtain information about intracellular biomolecules [3]. For instance, the surface plasmon resonance (SPR) technique has been successfully utilized to analyze the cell refractive index and study cell metabolic activities; however, the method still suffers from an extremely limited longitudinal detection range [4]. The terahertz (THz) wave, referring to the frequency band from 0.1 to 10 THz, locates between the microwave and infrared regions, and offers prominent advantages for biomedical applications, especially in the study of cells [5,6]. The dynamic process of bulk water occurs on a sub-picosecond to picosecond timescale. Hence, THz spectroscopy could be a unique method to characterize the intracellular hydration dynamics, which is closely related to cell biology and pathology processes [7,8]. Moreover, the energy of THz photons (i.e., ≈1–10 meV) is far below that of X-rays and cannot cause any ionization damage to organisms.

Although minute structural changes in the cell monolayer have been undoubtedly detected by conventional THz time-domain spectroscopy [9], the strong absorption of polar

#352263 https://doi.org/10.1364/BOE.10.001196
Journal © 2019 Received 19 Nov 2018; revised 28 Jan 2019; accepted 29 Jan 2019; published 11 Feb 2019

Biomedical Optics EXPRESS

liquids in the THz range still restricts their application to living cell monitoring. Recently, THz attenuated total reflection (ATR) spectroscopy has been successfully proposed to measure the complex dielectric responses of living cells in the culture medium [7,8,10,11]. In such a system, the penetration depth of the evanescent wave on the surface of the ATR prism corresponds to the thickness of the adherent cell monolayer, regardless of the weak effect of the upper solution. The cell monolayer should be cultured at the interface of the ATR prism *in situ*, with the help of a fixed incubation chamber to maintain a suitable environment. Interestingly, the ATR prism has been topped by a 3-mm-thick silicon (Si) patch for detection, which could be placed in the cell culture dish and covered with a cell monolayer [12]. However, small errors from the amplitude and phase shift, and angular misalignment of the prism may result in a significant variation in the measured complex dielectric constants [13].

THz metamaterials, composed of subwavelength periodic artificial metallic resonators, could couple the incident THz wave to enhance the localized electric field, particularly in the gap area; thus, they provide a highly sensitive sensing platform to detect biomolecules [14], nanovesicles [15], microorganisms [16] and cells [17]. The resonant feature (frequency and amplitude) will change even when a small number of targets fall within the enhanced near-field area of metamaterials. Depending on the concrete geometry of the design of the metamaterial, the detection range for target samples may go up to almost 3–4 μm and saturates at a particular film thickness of ~10 μm in the vertical direction [16,18]. A THz metamaterial-based sensing platform may acquire the whole cell monolayer response unlike an SPR-based technique. Cisplatin-induced cell apoptosis has been measured by a THz metamaterial-based biosensor in the transmission mode, with the results showing good correlation with those of flow cytometry analysis [17]. It has been noted that THz metamaterials could be easily placed into the common cell culture plate for cell biology research without any modifications. Nevertheless, the extracellular water is removed by dust-free paper in the measurement, as it may influence the vitality of living cells and not be suitable for continuous monitoring. Therefore, THz metamaterial-based reflection spectroscopy for living cell detection should be preferred.

In this study, we introduced the application of THz metamaterial-based reflection spectroscopy to extract the response of adherent living Madin–Darby canine kidney (MDCK) cells in phosphate buffered saline (PBS) solution. The self-referenced method—combined analysis of the reflection signals from Si undersurface and resonator/sample interface in one measurement—was utilized to simplify the measurement and reduce the phase shift error for real-time monitoring. Finite-difference time-domain (FDTD) simulations were conducted to verify the response of living MDCK cells, evaluate the feasibility of the proposed sensing method, and obtain the sensing performance for cellular dielectric property changes. Because of intracellular protein leakage, saponin-induced cell permeability change was also acquired as simulated. Furthermore, we also investigated the response of self-referenced signals for artificial cell density changes.

2. Materials and methods

2.1 Fabrication of THz metamaterial

The conventional photolithography method was used to fabricate the THz metamaterial sensors on a 550-μm-thick high-resistance Si substrate. 20-nm-thick chromium metal films and 200-nm-thick gold metal films were evaporated on the Si substrate successively. As shown in Fig. 1(a), we defined the resonator arrays of split square structures with a central gap on each side, which had a period of 70 μm, side width of 2 μm, gap size of 4 μm, and side length of 62 μm.

Biomedical Optics EXPRESS

2.2 Preparation of cell monolayer

MDCK cells, isolated from canine kidney, were obtained from ATCC, which would form a single-layer columnar epithelium with tight junctions when grown to confluence. The cells were cultured in Dulbecco's Modified Eagle Medium (DMEM) supplemented with 1% penicillin-streptomycin and 10% fetal bovine serum (all from Invitrogen Life Science, USA) at 37°C, 5% CO_2 condition, and harvested using 0.25% trypsin-EDTA within 5~10 min after washed with PBS solution. For sensing saponin-induced permeability changes, the cell suspension with a cell density of 1×10^6 cells/mL was seeded onto the surface of a clean THz metamaterial sensor (or bare Si wafer), and incubated for nearly 48 h until the cell monolayer formed and adhered tightly, as seen in Fig. 1(a). For quantitative measurements of the artificial cell density, various concentrations of cell suspension (2.5×10^5, 5×10^5, 7.5×10^5, and 1×10^6 cells/mL) were seeded onto the surface of four metamaterials, respectively, and incubated for 24 h. These four metamaterials were made in one batch with same resonance characteristics, which were verified by measuring the resonance peak in PBS solution. To obtain the average number of cells adhered to a single resonator (N_{avg}), we randomly chose 50 resonators located in the THz spot area and counted the adherent cell number on each side of the resonator by optical microscopy.

2.3 THz measurement of cells

Before THz measurements, the metamaterial (or bare Si wafer) attached with cells was taken out of the culture plate and washed with PBS solution lightly to get an intact cell monolayer on the surface. THz reflection spectroscopy was carried out on a commercial THz-TDS system (TAS7500SP, Advantest Corporation). The p-polarization collimated (the polarization direction perpendicular to the gap) THz wave was obliquely incident on the substrate side of the metamaterial (or bare Si wafer) with an incident angle of 10°, as illustrated in Fig. 1(b, c). The entire optical path was purged with dry air to exclude interference from water vapor. For sensing the cell monolayer, PBS solution was pipetted onto the cell monolayer, which reached a thickness of more than 1 mm, in order to keep the cells alive as well as exceed the penetration depth of THz waves [19]. After removing the adherent cell monolayer by 0.25% trypsin-EDTA, an equivalent PBS solution was added onto the sensor surface (or bare Si wafer) to acquire the THz signal. When analyzing saponin-induced cell permeability changes, two different concentrations (0.05% and 0.075% mass/volume) of saponin (Sigma Aldrich) and PBS solution were added onto identical metamaterial sensors covered with a cell monolayer, respectively. Real-time data acquisitions were made immediately; they lasted for 1 h with 2.5 min intervals. All THz measurements were performed at three different times under an ambient temperature of 25°C.

2.4 Self-referenced data analysis

The obtained THz time-domain waveforms of MDCK cell monolayers and PBS solution are shown in Fig. 2(a). Notably, the basic scheme of self-referenced data analysis in the reflected time-domain waveforms was as follows: the first pulse reflected from the Si undersurface was used as the reference signal and the second pulse reflected from the resonator/sample interface (or the Si wafer/sample interface) was used as the sample signal [20]. Thus, this self-referenced analysis method only needs a single measurement unlike the traditional reflection method, which requires a gold mirror signal as the reference signal. Thus, the self-referenced analysis method can simplify the measurement procedure and reduce the phase-shift error. Using fast Fourier transform for two pulses with a fixed time delay, the resulting frequency amplitudes for the sample were divided by that for the reference to get the characteristic self-referenced signals, which were all normalized to the signal for PBS solution on the metamaterial. As the more distinct discrepancy between the cell and PBS solution was the imaginary part of complex refractive index (discussed below), the intensity

Biomedical Optics EXPRESS

of the resonance peak (I_{peak}) in reflection signal was chosen to represent the modifications from different samples. For real-time monitoring, we defined relative signal variations Δ between initialized values of I_{peak} ($T = 0$) and reacting values of I_{peak} ($T = t$) at the monitoring moment of t as Eq. (1).

$$\Delta = \frac{I_{peak}(T=0) - I_{peak}(T=t)}{I_{peak}(T=0) - I_{peak}(\mathrm{PBS})} \tag{1}$$

2.5 FDTD simulation

In order to verify the experiment results, we utilized 3D-FDTD simulations (FDTD Solutions, Lumerical Solutions, Inc.) to simulate near-field enhanced electric field distribution and resonance in the THz metamaterial sensor on the Si substrate. Briefly, a linearly polarized plane wave with a frequency range of 0.1–3.5 THz was obliquely incident on the metamaterial with an incident angle of 10°. The geometric dimension for the metamaterial is the same as described in Section *2.1*. As the THz wave was obliquely incident on the period of metamaterial, Bloch boundary conditions were used in X and Y directions. The cell monolayer and PBS solution were treated as homogeneous media with two flat interfaces. Their complex refractive indexes were selected according to previous studies to mimic the experimental conditions as far as possible [7,21], whose imaginary parts were obviously different (e.g. ~0.65 for PBS solution and ~0.58 for cell monolayer at 1 THz) while real parts were indiscernible (e.g. ~2.14 for both PBS solution and cell monolayer at 1 THz). The chromium and gold metals can be treated as perfect electric conductor in simulations due to their high conductivity in the THz range. We selected 11 μm as the thickness of the MDCK cell monolayer for 3D-FDTD simulations, as shown in Fig. 2(b), due to the adherent MDCK cell monolayer staying at the height of 10~12μm [22]. The thickness-dependent response of the cell monolayer was investigated by changing the thickness of the cell monolayer with a constant PBS solution (~1000 μm) to confirm the effective vertical sensing range. The peak intensity variation (ΔV) was defined by Eq. (2). Meanwhile, we also analyzed the self-referenced signal variation in the cellular water content with various thicknesses of cell monolayers. All simulated time-domain waveforms were analyzed using the method mentioned above.

$$\Delta V = \frac{I_{peak}(\mathrm{cell}) - I_{peak}(\mathrm{PBS})}{I_{peak}(\mathrm{PBS})} \tag{2}$$

Biomedical Optics EXPRESS

3. Results and discussion

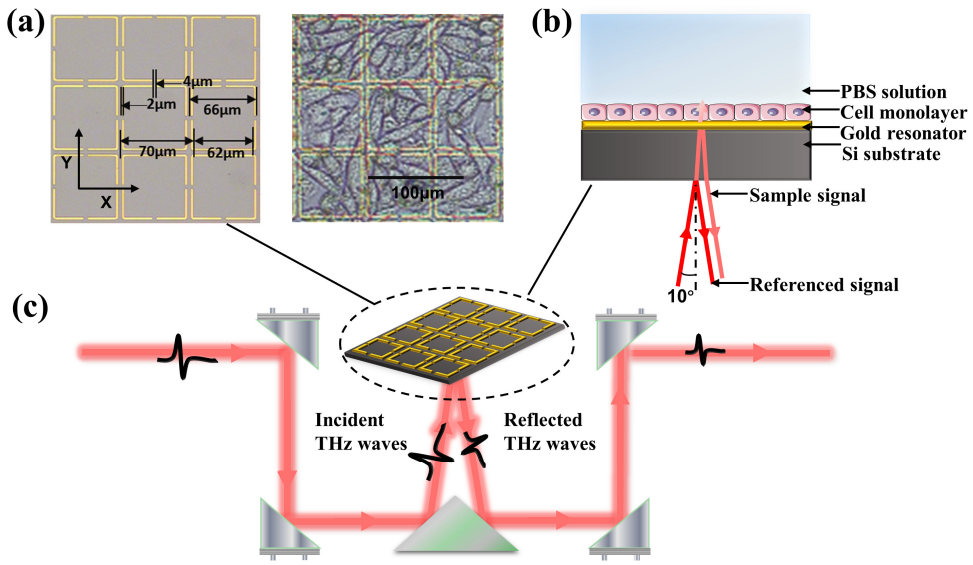

Fig. 1. (a) Optical micrograph of THz metamaterial sensor without (left) and with (right) MDCK cell monolayer; (b) schematic diagram of the self-referenced analysis of the living cell monolayer; (c) schematic diagram of the metamaterial-based reflection spectroscopy setup.

3.1 Self-referenced sensing of MDCK cell monolayer

As illustrated in Fig. 2(a), the first reflection pulses in the time-domain waveforms, ranging from 2 ps to 16 ps, were almost the same and were used as the reference signal. Meanwhile, the second reflection pulses, ranging from 16 ps to 30 ps, are distinctive for the adherent MDCK cell and PBS solution, which carry the information about the sample upon the gold resonator interface. The self-referenced signals of the MDCK cell and PBS solution (in Fig. 2(b)) show prominent resonance peaks close to 0.9 THz, yielding a significant intensity variation (~0.115) but a slight frequency shift. In other words, the self-referenced resonance peak for the MDCK cell becomes broader and higher than that for PBS solution, whose frequency shift could hardly be determined. However, tiny variations (~0.013 at 0.9 THz) were observed on the bare Si wafer without any resonant structures. Thus, we could obtain nearly 9 times enhancement benefit owing to strong interactions of the highly confined electric field of the metamaterial with the adherent cell monolayer. The simulated reflection spectra, obtained by 3D-FDTD simulations and self-referenced analysis, correlated well with the experimental results.

According to the inductor–capacitor resonance mode, variations in the complex refractive index of samples appearing on the metamaterial surface would change the shift and intensity of the resonance peak [19]. Previous simulation results have shown that increasing the refractive index will alter the resonance frequency far beyond the peak intensity, whereas the changed extinction coefficients only influence the resonance peak intensity [23]. The imaginary part of the complex refractive index of living cells was lower than distilled water, far beyond the discrepancy between their real parts, due to the replacement of a portion of strongly absorbing bulk water by intracellular biomolecules and hydrated water [7]. Here, the tendency of variation of the reflection peak intensity for the different imaginary parts (those of living cells and PBS solution) was in line with previous observations made using a similar method in an ethanol/water mixture [20], and the results were further verified by 3D-FDTD simulations. Although the reflection peak intensity of the self-referenced signal could not

Biomedical Optics EXPRESS

gain the definite value of dielectric response, it still carried information about the imaginary part of the complex refractive index of the adherent cell monolayer and can be a suitable indicator for monitoring particularly intracellular water dynamics. While the thickness of the cell monolayer will vary for different kinds of cells, we should evaluate the feasibility of this metamaterial-based living cell sensing concept by investigating the thickness-dependent effect of the cell monolayer.

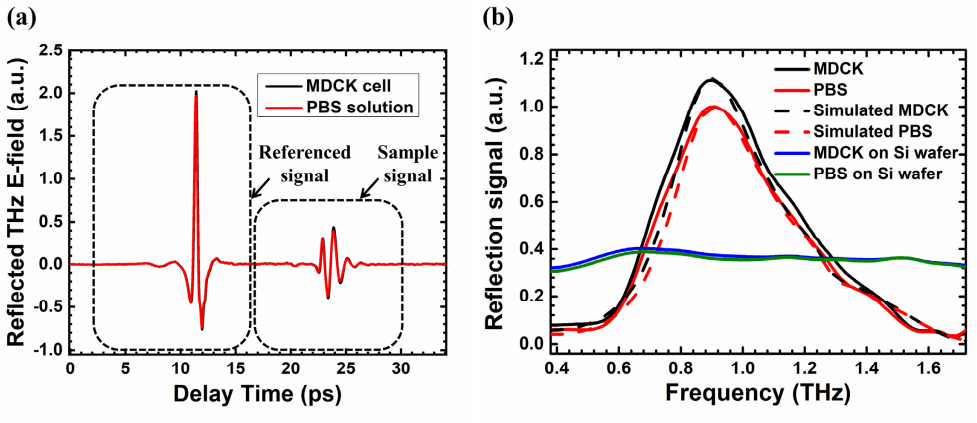

Fig. 2. (a) Reflective THz time-domain waveforms and (b) normalized simulated (dashed line) and experimental (solid line) reflection spectra for self-referenced sensing of PBS solution (~1000 μm in simulation) and living MDCK cell in PBS solution (~11-μm-thick cell monolayer and 1000-μm-thick PBS solution in simulation) on the metamaterial (black for cell and red for PBS solution) and on the Si wafer (blue for cell and olive for PBS solution).

3.2 Feasibility of living cell sensing by THz metamaterial

We simulated the THz metamaterial-based response of the cell monolayer in a representative thickness range (0–20.5 μm) with a fixed upper PBS solution layer (~1000 μm), the thickness of which is greater than the penetration depth of incident THz waves, as shown in Fig. 3(a). The resonance peak intensity variations and electric field distribution were determined and plotted in Fig. 3(b). Apparently, the resonance peak intensity increased with the thickness of the adherent cell monolayer, and started to saturate at a thickness of 5.5 μm. The electric field distribution, caused by a spoof surface plasma [24], was highly confined on the surface and weakened above the space perpendicular to the metamaterial. Moreover, the z-cut along the direction of propagation demonstrated the localized electric field decayed exponentially to 1/*e* of its maximum at the vertical height of ~1.5 μm, signifying a significant change in the resonance peak intensity when the simulated cell monolayer thickness was below 2.5 μm. The intensity of the electric field continued to decrease gradually till the vertical height of nearly 7~8 μm, in accordance with the saturated behavior of cell monolayer. Notably, typical adherent cell monolayers, whose thickness were in a range of 5.5–13 μm [7,22], occupied almost all of the electric field distribution area, and then did not further modify the resonance peak intensity and became immune to any contribution from the upper PBS solution layer. Thus, given that most adherent cell monolayers are accidented with protuberant nucleus as well as flat cytoplasm, this metamaterial-based cell sensing platform is also unaffected by thickness variation of cell monolayers. For future cell monitoring applications, we need to further assess the sensing performance of metamaterials for dielectric property changes (e.g., water content variation) of the cell monolayer.

Biomedical Optics EXPRESS

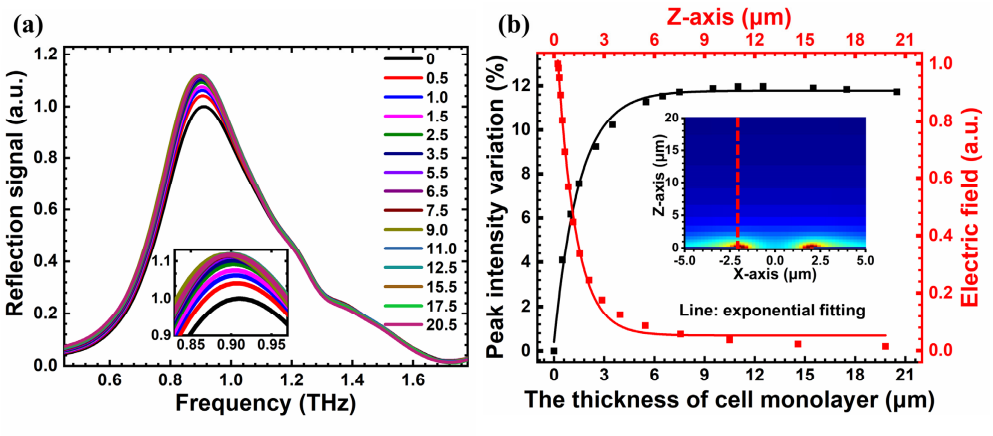

Fig. 3. Normalized reflection spectra of thickness-dependent cell monolayer for self-referenced sensing of living MDCK cell. (a) Simulated results with the thickness of cell monolayer ranging from 0 μm to 20.5 μm. (b) Peak intensity variation as a function of the change of cell monolayer thickness, and electric field profiles along z-axis at the positions indicated by red dotted lines in the inset. The solid lines are the exponential fitting. Inset in Fig. 3(b) shows the simulated electric field maps at the resonant frequency for the gap area (corresponds to the range of –2 μm to 2 μm on the x-axis) of the used THz metamaterial with no adherent dielectric material but air.

3.3 Monitoring of saponin-induced cell permeability change

Water, termed as "an active matrix of life for cell biology", plays a vital role in enabling the functions of intracellular biomolecules and assisting chemical interactions and information transfer processes within the cell [25]. Intracellular water could be classified as osmotically unresponsive hydrated water, confined in the vicinity of biomolecules, and free-flowing bulk water, which promotes the fluidity of cytoplasm, thus altering the cellular metabolic process. Therefore, water content (i.e., bulk water) of the cell monolayer is closely related to the cellular activity and pathological state [8]. We selected the water content variation of the cell monolayer as the indicator in our simulations, which was based on the assumption that the cell monolayer is approximately non-dispersive [17] and additional bulk water content variation ($\Delta_{water\ content}$) of the cell monolayer would mainly lead to a change in the imaginary part of its complex refractive index according to a two-component model [26]: $\kappa_{altered\ cell} = \kappa_{cell} + \Delta_{water\ content} \times (\kappa_{PBS} - \kappa_{cell})$, where κ_{PBS} and κ_{cell} refer to the aforementioned imaginary part of the complex refractive index (i.e., extinction coefficient) of the PBS solution and cell monolayer, respectively. As illustrated in Fig. 4(a), the relative variation in the self-referenced signal rises linearly with the $\Delta_{water\ content}$, until the simulated cell monolayer completely transforms into a simulated PBS solution layer (i.e., $\Delta_{water\ content} = 100\%$) . The self-referenced resonance peak intensity is mainly dependent on the imaginary part of the complex refractive index of the adjacent object, and would thus respond to any changing adjacent circumstances. In particular, a nearly identical relative signal variation tendency was observed with an outstanding linearity when simulating cell monolayers with different thicknesses as the $\Delta_{water\ content}$ changed. Therefore, we deem that this metamaterial-based cell sensor can monitor changes in the cellular dielectric properties caused by intracellular water content or even other intrinsic characteristics changes, independent of the thickness of the cell monolayer.

Saponin, known as a nonionic detergent, can permeate living or fixed cells at different concentrations [27,28], and is widely used in immunocytochemistry and flow cytometry for the detection of intracellular biomolecules [29]. It can selectively bind with membrane

cholesterol and produce tiny pores in cell membranes without any destruction [30,31]. These pores allow diffusion of water molecules and component exchange between intracellular and extracellular environments, and generally enhance the cell membrane permeability. The monitoring of saponin-induced cell permeability changes was carried out as shown in Fig. 4(b). When saponin was added at 0 min, the relative signal variations Δ began to decrease a bit, and then turned to increase at 7.5 min for 0.075% saponin and 15 min for 0.05% saponin, and finally reached the value of nearly 0.8 for 0.075% saponin and 0.4 for 0.05% saponin. The curves for cells immersed in the same amount of PBS solution (PBS control) show no obvious variations but only tiny fluctuations. The cell monolayer, observed by optical microscopy, remained on the surface of metamaterial without obvious detachment throughout the monitoring period, which verified the origin of signal variation. These results are in good agreement with previous results obtained using THz-ATR spectroscopy, which implies the saponin-induced THz contrast change to be due to intracellular protein leakage [12]. However, this metamaterial-based cell sensor is simpler and more portable. Akin to the variation tendency seen in the simulations for cellular water content change, relative signal variations Δ rose and became close to the background signal of the PBS solution as the interaction of saponin went on, indicating the profound permeability change of cell monolayer. Owing to the concentration-dependent manner of the saponin-induced permeability change [32], the Δ for 0.075% saponin rose faster and achieved a bigger change than 0.05% saponin. The initial plateau (slightly reduced Δ at the beginning) for 0.075% remained almost twice as short for 0.05% saponin (7.5 min versus 15 min), as was required for the extensive interaction between saponin and the cell membrane, so that component exchange can take place. In general, this metamaterial-based cell sensor could real-timely probe saponin-induced cell permeability changes in a label-free as well as self-referenced manner, which is useful in tumor cytopathology because of the high water content of tumor cells [33].

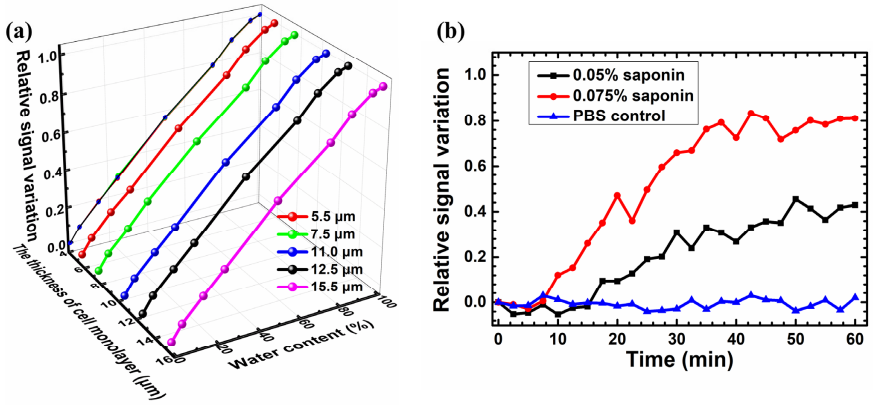

Fig. 4. (a) Simulated THz self-referenced reflection spectra for thickness-dependent cell monolayer (5.5 μm, 7.5 μm, 11.0 μm, 12.5 μm, and 15.5 μm) with the water content ranging from 0% to 100% and a fixed upper PBS solution layer (1000 μm) and (b) relative signal variation versus time for monitoring living MDCK cell monolayer after exposure to PBS solution and 0.05% and 0.075% saponin.

3.4 Measurement of adherent cell number change

Apart from the concern about changes in the cellular dielectric properties, cell counting, either as the ultimate purpose or as a critical intermediate step, is also indispensable for most cell biology research [34]. Taking transwell assay as an instance, the ability of cell migration or invasion could be evaluated by analyzing the cell number in the lower part of the porous membrane (i.e., cell density distribution) [35]. Owing to various seeding concentrations of the cell suspension, four identical metamaterials with diverse artificial cell density

Biomedical Optics EXPRESS

distributions were obtained, as seen in insets of Fig. 5(a-d). Meanwhile, the peak intensity of the self-referenced signal increased gradually with augmenting of the adherent cell density, demonstrating a marked linearity with a linear correlation coefficient (R^2) of 0.9914, as shown in Fig. 5(e). It is obvious that decrease in the cell density would lead to increase in the amount of extracellular water, which fills the interstitial space, thus altering the nearby dielectric environment. Based on the equivalent medium theory [17] and the above-mentioned assumption, we considered any cells together with extracellular water located at the effective sensing range as a non-dispersively equivalent cell monolayer, whose dielectric property correlated to the cell number, and assigned the peak intensity variation to changes in the water content of this equivalent cell monolayer. Given that the saturated cell density corresponds to N_{avg} = 6.83, the exceeding 20% of saturated peak intensity variation (~0.026 versus 0.115) at a lower cell density of N_{avg} = 1.27, refers to nearly 80% occupation of extracellular water in equivalent cell monolayer (~1.27 versus 6.83). This result correlates well with aforementioned simulation results in Fig. 4(a), where 20% of the saturated peak intensity variation was attributed to 78% of the water content change. Although this is no more than a preliminary result, it strongly suggests that the metamaterial-based cell sensor could effectively respond to adherent cell density change on account of extracellular water change, which is promising for the development of a novel cell-counting method without the need of labels.

There are several advantages for our proposed metamaterial-based cell sensing platform. First, with the aid of THz metamaterial-based reflection spectroscopy, we can obtain signals for living adherent cell monolayers, and effectively sense changes in the cellular dielectric properties and cell density: this is similar to the THz-ATR methodology but is more compact and easier to integrate. Secondly, it can acquire more in-depth information about the cell monolayer up to a micron level unlike SPR methods. Finally, owing to the relatively polarization-insensitive design with the only requirement being the polarization direction of the incident THz wave having to be perpendicular to any gap, and the use of a self-referenced method, this method is convenient for practical measurements and avoids phase shift errors caused by the misplacement between the metamaterial and reference gold mirror [36]. Further improvement of this sensing platform is required, such as including highly hydrophilic substrate [15], low dielectric constant of substrate [37], novel resonance structure (e.g., Fano resonance) [38], and targeted enhancement nanomaterials (e.g., conjugated avidin-gold nanoparticles with a high refractive index) [23].

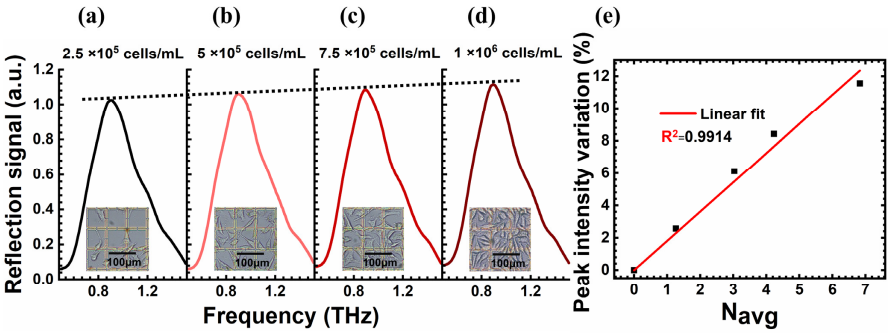

Fig. 5. (a-d) Normalized self-referenced reflection spectra for various seeding concentrations of cell suspension (2.5 × 10^5, 5 × 10^5, 7.5 × 10^5, and 1 × 10^6 cells/mL) on metamaterial surface. Insets are optical micrographs of the metamaterial with different cell densities corresponding to various seeding concentrations. (e) The plot of peak intensity variation as a function of changes in average cell number adhered to a single resonator (N_{avg}). The red line is a linear fit for the N_{avg} and peak intensity variation.

Biomedical Optics EXPRESS

4. Conclusion

In summary, THz metamaterial-based reflection spectroscopy was used for living cell sensing in a self-referenced method. Due to the strong localized electric field enhancement of the metamaterial, the resonance peak intensity of the self-referenced signal, corresponding to the imaginary part of the complex refractive index of the adherent target, demonstrates obvious differences between the MDCK cell monolayer and PBS solution through experiments and simulations. The proposed cell sensor is unaffected by thickness deviation in living cells and shows saturated response behavior in liquid phase. The relative variations in the self-referenced signal show a linear dependence with changes in the dielectric property (e.g., water content) of the cell monolayer as the simulated results, irrespective of the cell thickness. Further verification of the proposed metamaterial sensor by real-time monitoring of saponin-induced cell permeability change correlates well with previous results obtained by THz-ATR experiments and simulations. Moreover, adherent cell density alterations could be appropriately evaluated due to changes in the extracellular water content. It should be noted that our sensing platform offers the additional benefits of a convenient THz living cell sensor setup, a sensing range of up to the whole cell monolayer, and inherent stability of the self-referenced method. Further research will focus on optimizing this cell sensor and integrating it into common cell culture plates for label-free, *in situ* analysis of cellular proliferation, differentiation, apoptosis, and interactions.

Funding

National Basic Research Program of China (Program 973) (2015CB755400); National Natural Science Foundation of China (NSFC) (81430054, 81802118); Military Logistics Application Basic Research Project (AWS17J010); Natural Science Foundation of Chongqing, China (cstc2017jcyjB0142).

Disclosures

The authors declare that there are no conflicts of interest related to this article.

References

1. G. Bao and S. Suresh, "Cell and molecular mechanics of biological materials," Nat. Mater. **2**(11), 715–725 (2003).
2. N. Yu, J. M. Atienza, J. Bernard, S. Blanc, J. Zhu, X. Wang, X. Xu, and Y. A. Abassi, "Real-time monitoring of morphological changes in living cells by electronic cell sensor arrays: an approach to study G protein-coupled receptors," Anal. Chem. **78**(1), 35–43 (2006).
3. P. Y. Liu, L. K. Chin, W. Ser, H. F. Chen, C. M. Hsieh, C. H. Lee, K. B. Sung, T. C. Ayi, P. H. Yap, B. Liedberg, K. Wang, T. Bourouina, and Y. Leprince-Wang, "Cell refractive index for cell biology and disease diagnosis: past, present and future," Lab Chip **16**(4), 634–644 (2016).
4. L. X. Sun, Y. Q. Zhang, Y. J. Wang, C. L. Zhang, C. J. Min, Y. Yang, S. W. Zhu, and X. C. Yuan, "Refractive index mapping of single cells with a graphene-based optical sensor," Sens. Actuators B Chem. **242**, 41–46 (2017).
5. X. Yang, X. Zhao, K. Yang, Y. Liu, Y. Liu, W. Fu, and Y. Luo, "Biomedical Applications of Terahertz Spectroscopy and Imaging," Trends Biotechnol. **34**(10), 810–824 (2016).
6. X. Yang, D. Wei, S. Yan, Y. Liu, S. Yu, M. Zhang, Z. Yang, X. Zhu, Q. Huang, H. L. Cui, and W. Fu, "Rapid and label-free detection and assessment of bacteria by terahertz time-domain spectroscopy," J. Biophotonics **9**(10), 1050–1058 (2016).
7. K. Shiraga, Y. Ogawa, T. Suzuki, N. Kondo, A. Irisawa, and M. Imamura, "Characterization of dielectric responses of human cancer cells in the terahertz region," J. Infrared Millim. Terahertz Waves **35**(5), 493–502 (2014).
8. K. Shiraga, T. Suzuki, N. Kondo, K. Tanaka, and Y. Ogawa, "Hydration state inside HeLa cell monolayer investigated with terahertz spectroscopy," Appl. Phys. Lett. **106**(25), 253701 (2015).
9. H. B. Liu, G. Plopper, S. Earley, Y. Chen, B. Ferguson, and X. C. Zhang, "Sensing minute changes in biological cell monolayers with THz differential time-domain spectroscopy," Biosens. Bioelectron. **22**(6), 1075–1080 (2007).
10. K. Shiraga, Y. Ogawa, T. Suzuki, N. Kondo, A. Irisawa, and M. Imamura, "Determination of the complex dielectric constant of an epithelial cell monolayer in the terahertz region," Appl. Phys. Lett. **102**(5), 053702 (2013).

Biomedical Optics EXPRESS

11. Y. Zou, Q. Liu, X. Yang, H. C. Huang, J. Li, L. H. Du, Z. R. Li, J. H. Zhao, and L. G. Zhu, "Label-free monitoring of cell death induced by oxidative stress in living human cells using terahertz ATR spectroscopy," Biomed. Opt. Express **9**(1), 14–24 (2018).
12. M. Grognot and G. Gallot, "Quantitative measurement of permeabilization of living cells by terahertz attenuated total reflection," Appl. Phys. Lett. **107**(10), 103702 (2015).
13. A. Soltani, T. Probst, S. F. Busch, M. Schwerdtfeger, E. Castro-Camus, and M. Koch, "Error from delay drift in terahertz attenuated total reflection spectroscopy," J. Infrared Millim. Terahertz Waves **35**(5), 468–477 (2014).
14. D. K. Lee, J. H. Kang, J. S. Lee, H. S. Kim, C. Kim, J. H. Kim, T. Lee, J. H. Son, Q. H. Park, and M. Seo, "Highly sensitive and selective sugar detection by terahertz nano-antennas," Sci. Rep. **5**(1), 15459 (2015).
15. D. K. Lee, H. Yang, H. S. Song, B. Park, E.-M. Hur, J. H. Kim, T. H. Park, and M. Seo, "Ultrasensitive terahertz molecule sensor for observation of photoinduced conformational change in rhodopsin-nanovesicles," Sens. Actuators B Chem. **273**, 1371–1375 (2018).
16. S. J. Park, J. T. Hong, S. J. Choi, H. S. Kim, W. K. Park, S. T. Han, J. Y. Park, S. Lee, D. S. Kim, and Y. H. Ahn, "Detection of microorganisms using terahertz metamaterials," Sci. Rep. **4**(1), 4988 (2015).
17. C. Zhang, L. Liang, L. Ding, B. Jin, Y. Hou, C. Li, L. Jiang, W. Liu, W. Hu, Y. Lu, L. Kang, W. Xu, J. Chen, and P. Wu, "Label-free measurements on cell apoptosis using a terahertz metamaterial-based biosensor," Appl. Phys. Lett. **108**(24), 241105 (2016).
18. S. J. Park, S. A. N. Yoon, and Y. H. Ahn, "Dielectric constant measurements of thin films and liquids using terahertz metamaterials," RSC Advances **6**(73), 69381–69386 (2016).
19. F. Miyamaru, K. Hattori, K. Shiraga, S. Kawashima, S. Suga, T. Nishida, M. W. Takeda, and Y. Ogawa, "Highly sensitive terahertz sensing of glycerol-water mixtures with metamaterials," J. Infrared Millim. Terahertz Waves **35**(2), 198–207 (2014).
20. X. Wu, X. Pan, B. Quan, X. Xu, C. Gu, and L. Wang, "Self-referenced sensing based on terahertz metamaterial for aqueous solutions," Appl. Phys. Lett. **102**(15), 151109 (2013).
21. X. Zhao, M. Zhang, D. Wei, Y. Wang, S. Yan, M. Liu, X. Yang, K. Yang, H. L. Cui, and W. Fu, "Label-free sensing of the binding state of MUC1 peptide and anti-MUC1 aptamer solution in fluidic chip by terahertz spectroscopy," Biomed. Opt. Express **8**(10), 4427–4437 (2017).
22. A. Puliafito, L. Hufnagel, P. Neveu, S. Streichan, A. Sigal, D. K. Fygenson, and B. I. Shraiman, "Collective and single cell behavior in epithelial contact inhibition," Proc. Natl. Acad. Sci. U.S.A. **109**(3), 739–744 (2012).
23. W. D. Xu, L. J. Xie, J. F. Zhu, X. Xu, Z. Z. Ye, C. Wang, Y. G. Ma, and Y. B. Ying, "Gold nanoparticle-based terahertz metamaterial sensors: mechanisms and applications," ACS Photonics **3**(12), 2308–2314 (2016).
24. J. B. Pendry, L. Martín-Moreno, and F. J. Garcia-Vidal, "Mimicking surface plasmons with structured surfaces," Science **305**(5685), 847–848 (2004).
25. P. Ball, "Water is an active matrix of life for cell and molecular biology," Proc. Natl. Acad. Sci. U.S.A. **114**(51), 13327–13335 (2017).
26. Y. Sun, Y. Zhang, and E. Pickwell-Macpherson, "Investigating Antibody Interactions with a Polar Liquid Using Terahertz Pulsed Spectroscopy," Biophys. J. **100**(1), 225–231 (2011).
27. E. Weibull, S. Matsui, M. Sakai, H. Andersson Svahn, and T. Ohashi, "Microfluidic device for generating a stepwise concentration gradient on a microwell slide for cell analysis," Biomicrofluidics **7**(6), 064115 (2013).
28. K. Medepalli, B. W. Alphenaar, R. S. Keynton, and P. Sethu, "A new technique for reversible permeabilization of live cells for intracellular delivery of quantum dots," Nanotechnology **24**(20), 205101 (2013).
29. M. C. Jacob, M. Favre, and J. C. Bensa, "Membrane cell permeabilization with saponin and multiparametric analysis by flow cytometry," Cytometry **12**(6), 550–558 (1991).
30. G. Francis, Z. Kerem, H. P. S. Makkar, and K. Becker, "The biological action of saponins in animal systems: a review," Br. J. Nutr. **88**(6), 587–605 (2002).
31. M. C. Jamur and C. Oliver, "Permeabilization of Cell Membranes," in *Immunocytochemical Methods and Protocols*, C. Oliver, and M. C. Jamur, ed. (Humana Press, Totowa, NJ, 2010), pp. 63–66.
32. M. Wassler, I. Jonasson, R. Persson, and E. Fries, "Differential permeabilization of membranes by saponin treatment of isolated rat hepatocytes. Release of secretory proteins," Biochem. J. **247**(2), 407–415 (1987).
33. S. Sy, S. Huang, Y. X. J. Wang, J. Yu, A. T. Ahuja, Y. T. Zhang, and E. Pickwell-MacPherson, "Terahertz spectroscopy of liver cirrhosis: investigating the origin of contrast," Phys. Med. Biol. **55**(24), 7587–7596 (2010).
34. E. Primiceri, M. S. Chiriacò, R. Rinaldi, and G. Maruccio, "Cell chips as new tools for cell biology--results, perspectives and opportunities," Lab Chip **13**(19), 3789–3802 (2013).
35. Y. Wang, X. Zeng, N. Wang, W. Zhao, X. Zhang, S. Teng, Y. Zhang, and Z. Lu, "Long noncoding RNA DANCR, working as a competitive endogenous RNA, promotes ROCK1-mediated proliferation and metastasis via decoying of miR-335-5p and miR-1972 in osteosarcoma," Mol. Cancer **17**(1), 89 (2018).
36. Y. Zhang, L. Zhang, P. Sun, Y. He, Y. Zou, and Y. Deng, "Extracting Complex Refractive Index from Polycrystalline Glucose with Self-Referenced Method for Terahertz Time-Domain Reflection Spectroscopy," Appl. Spectrosc. **70**(7), 1102–1108 (2016).
37. X. Wu, B. Quan, X. Pan, X. Xu, X. Lu, C. Gu, and L. Wang, "Alkanethiol-functionalized terahertz metamaterial as label-free, highly-sensitive and specific biosensor," Biosens. Bioelectron. **42**, 626–631 (2013).
38. I. Al-Naib, C. Jansen, R. Singh, M. Walther, and M. Koch, "Novel THz Metamaterial Designs: From Near- and Far-Field Coupling to High-Q Resonances," IEEE Trans. Terahertz Sci. Technol. **3**(6), 772–782 (2013).